

# Electrostatic energy of Coulomb crystals with polarized electron background\*

A. A. Kozhberov<sup>†</sup> and A. Y. Potekhin<sup>‡</sup>

*Ioffe Institute, Politekhnikeskaya 26, Saint Petersburg, 194021, Russia*

(Dated: April 21, 2021)

Outer crusts of neutron stars and interiors of cool white dwarfs consist of bare atomic nuclei, arranged in a crystal lattice and immersed in a Fermi gas of degenerate electrons. We study electrostatic properties of such Coulomb crystals, taking into account the polarizability of the electron gas and considering different structures, which can form the ground state: body-centered cubic (bcc), face-centered cubic (fcc), hexagonal close-packed (hcp), and MgB<sub>2</sub>-like lattices. At zero temperature the electrostatic energy brings a fundamental contribution to the total energy of the classical Coulomb crystal, which allows us to study structural transitions in the neutron-star crusts and crystallized white-dwarf interiors. To take the electron background polarization into account, we use the linear response theory with the electron dielectric function given either by the Thomas-Fermi approximation or by the random-phase approximation (RPA). We compare the widely used nonrelativistic (Lindhard) version of the RPA approximation with the more general, relativistic (Jancovici) version. The results of the different approximations are compared to assess the importance of going beyond the Thomas-Fermi or Lindhard approximations. We also include contribution of zero-point vibrations of ions into the ground-state energy. We show that the bcc lattice forms the ground state for any charge number  $Z$  of the atomic nuclei at the densities where the electrons are relativistic ( $\rho \gtrsim 10^6$  g cm<sup>-3</sup>), while at the nonrelativistic densities ( $\rho \lesssim 10^6$  g cm<sup>-3</sup>) the fcc and hcp lattices can form the ground state. The MgB<sub>2</sub>-like lattice never forms the ground state at realistic densities in the crystallized regions of degenerate stars. The RPA corrections strongly affect the boundaries between the phases. As a result, transitions between different ground-state structures depend on  $Z$  in a nontrivial way. The relativistic and quantum corrections produce less dramatic effects, moderately shifting the phase boundaries.

**PACS numbers** 52.27.Gr, 52.27.Lw, 52.25.Kn, 05.70.Ce

## I. INTRODUCTION

A model of Coulomb plasma assumes that the system consists of point-like charged particles and the neutralizing background. The basic physics behind this model was explored in many works and summarized in a number of review papers, textbooks and monographs (e.g., [1–3], and references therein). This model is quite universal and is used in many areas of physics, for example, in astrophysics, for description of such different objects as neutron stars, white dwarfs, gas giants, and dusty clouds (e.g., [4–10]).

At sufficiently low temperatures or high densities, the Coulomb plasma forms a crystal (see, e.g., Ref. [11] for a discussion of the phase diagram of Coulomb crystals in classical and quantum plasmas). In particular, some regions of the degenerate stars, namely crusts of neutron stars (e.g., [9], and references therein) and cores of sufficiently cool white dwarfs (e.g., [9, 12], and references therein), are formed by Coulomb crystals, where a lattice of bare atomic nuclei is embedded in the background of degenerate electrons. The question, which type of crystal lattice forms in such stars, is not solved completely. For crystals with the same ion charge number  $Z$  it was

discussed in [9, 13–15]. More complex systems with two or three different charged ions were studied in [14–17]. In all of the papers cited above, the uniform electron background was considered.

The aim of the present paper is to take into account the influence of the electron background polarization on the electrostatic energy and the ground state of a Coulomb crystal. Previously this problem was studied only for the body-centered cubic (bcc) and face-centered cubic (fcc) lattices [1, 18–21]. In this paper, we investigate other lattices, such as hexagonal close-packed (hcp) and one-component MgB<sub>2</sub>. It allows us to construct a more complete picture of structural transitions in degenerate stars. As well as the previous authors, we assume that the electron screening is weak, which is justified in the case of strongly degenerate electrons. We consider different lattices, calculate their ground-state energies, and find which lattice is most preferable. The electron polarization effects are described in frames of the linear response theory by the dielectric function, for which we use and compare three approximations: the widely used Thomas-Fermi theory, the Lindhard model [22] based on the non-relativistic random-phase approximation (RPA), and the extension of the Lindhard model for the relativistic electrons [23] (see also, e.g., [1, 24]). Comparing the results obtained using these three models, we will estimate the importance of the corrections beyond the Thomas-Fermi approximation and of the effects of special relativity.

The paper is organized as follows. In Sec. II we introduce basic parameters of the polarized electron back-

\*Published in *Phys. Rev. E* **103**, 043205 (2021),  
<https://doi.org/10.1103/PhysRevE.103.043205>

<sup>†</sup>Electronic address: kozhberov@gmail.com

<sup>‡</sup>Electronic address: palex@astro.ioffe.ru

ground and present the three different approximations for the dielectric function, which are used in the subsequent sections. In Sec. III we determine the ground state structure of the Coulomb plasma, following the approach of Chamel and Fantina [14]. According to this approach, at zero temperature the type of the lattice is mainly determined by the electrostatic energy, all point-like ions being in equilibrium positions  $\mathbf{R}_l$ . We compute the electrostatic energy in different approximations and compare the results for the phase boundaries between different ground-state structures. In Sec. IV we go beyond the approach of Chamel and Fantina [14] by taking into account the zero-point vibrations of ions around their equilibrium positions. In Sec. V we check the accuracy of the calculated ground-state energy and positions of phase boundaries by evaluation of possible corrections to our approximations. Results are discussed and conclusions are given in Sec. VI.

## II. PARAMETERS AND APPROXIMATIONS FOR POLARIZED BACKGROUND

Since ions move slowly, it is sufficient to use the linear response approximation and the static longitudinal dielectric function  $\epsilon(q)$  to describe the degenerate electron background [25]. In the approximation of the uniform (“rigid”) background,  $\epsilon(q) = 1$ . In the present paper we take the background nonuniformity into account by considering only the first-order perturbation corrections to the dielectric function  $\epsilon(q)$ . It is convenient to write

$$\epsilon(q) = 1 + \frac{\kappa_{\text{TF}}^2}{q^2} \epsilon_2(q), \quad (1)$$

where  $q$  is the wavenumber,  $\epsilon_2(q)$  is the correction, which will be discussed later, and

$$\kappa_{\text{TF}} = \sqrt{4\pi e^2 \frac{\partial n_e}{\partial \mu_e}} \approx 2\sqrt{\frac{e^2}{\pi \hbar v_F} \frac{p_F}{\hbar}} \quad (2)$$

is the Thomas-Fermi electron wavenumber. Here,  $n_e$  is the electron number density,  $\mu_e$  is the electron chemical potential,  $p_F = \hbar(3\pi^2 n_e)^{1/3}$  is the Fermi momentum, and  $v_F = \partial E_F / \partial p_F$  is the Fermi velocity,  $E_F$  being the Fermi energy. The first equality in Eq. (2) is quite general, while the second is approximately valid in the case of strongly degenerate electrons, where  $\mu_e \approx E_F$ .

In the degenerate stars, the electrons can be relativistic due to high densities. The relativity parameter [26] is

$$x \equiv \frac{p_F}{m_e c} \approx 0.01 (\rho Z/A)^{1/3}, \quad (3)$$

where  $m_e$  is the electron mass,  $\rho$  is mass density in units of  $\text{g cm}^{-3}$ ,  $Z$  is the ion charge number and  $A$  is the relative atomic weight of the considered isotope. The second part of Eq. (3) assumes the neutrality condition  $n_e = Zn$ , where  $n$  is the ion number density.

In plasma physics, it is customary to use the dimensionless density parameter  $r_s = a_e/a_B$ , where  $a_e = (4\pi n_e/3)^{-1/3}$  is the electron sphere radius and  $a_B \equiv \hbar^2/m_e e^2$  is the Bohr radius. It is related to the relativity parameter as  $r_s = (9\pi/4)^{1/3} \alpha/x \approx 0.014/x$ , where  $\alpha \equiv e^2/\hbar c$  is the fine structure constant.

In general, Eq. (2) is valid both for the nonrelativistic treatment and for the special relativity taken into account. In the latter case, Eq. (2) leads to the expression

$$\kappa_{\text{TF}} a_e = \left(\frac{18}{\sqrt{\pi}}\right)^{1/3} \sqrt{\frac{\alpha\gamma}{x}} \approx 0.185 \sqrt{\frac{\gamma}{x}}, \quad (4)$$

where  $\gamma \equiv \sqrt{1+x^2}$  is the electron Lorentz factor on the Fermi surface.

The importance of the electron polarization is mainly indicated by the Thomas-Fermi parameter  $\kappa_{\text{TF}} a$ , where  $a \equiv (4\pi n/3)^{-1/3}$  is the ion sphere radius. The charge neutrality requires that  $a = a_e Z^{1/3}$ , and then Eq. (4) yields

$$\kappa_{\text{TF}} a \approx 0.185 Z^{1/3} \sqrt{\frac{\gamma}{x}}. \quad (5)$$

The model of uniform electron background is equivalent to neglecting the term with  $\epsilon_2(q)$  in Eq. (1). To go beyond this approximation, we use three expressions for  $\epsilon_2(q)$ . The most common of them is the Thomas-Fermi approximation, which is valid in the long-distance (short wavenumber) limit at any  $x$ . It gives

$$\epsilon_{2\text{TF}}(q) = 1. \quad (6)$$

In the non-relativistic case ( $x \ll 1$ ) and for strongly degenerate electrons, the RPA leads to the Lindhard (L) dielectric function [22],

$$\epsilon_{2\text{L}}(q) = \frac{1}{2} + \frac{1-y^2}{4y} \ln \left| \frac{1+y}{1-y} \right|. \quad (7)$$

where  $y = \hbar q/(2p_F) \approx 0.26 q a_e$ .

The RPA with allowance for the electron relativity leads to the Jancovici (J) model [23]

$$\begin{aligned} \epsilon_{2\text{J}}(q) = & \frac{2}{3} - \frac{2}{3} \frac{y^2 x}{\gamma} \ln(x+\gamma) + \frac{x^2+1-3x^2 y^2}{6yx^2} \ln \left| \frac{1+y}{1-y} \right| \\ & + \frac{2y^2 x^2 - 1}{6yx^2} \frac{\sqrt{1+x^2 y^2}}{\gamma} \ln \left| \frac{y\gamma + \sqrt{1+x^2 y^2}}{y\gamma - \sqrt{1+x^2 y^2}} \right|. \end{aligned} \quad (8)$$

The Jancovici dielectric function reduces to the Lindhard dielectric function in the nonrelativistic limit  $x \rightarrow 0$ , and both Lindhard and Jancovici models reduce to the Thomas-Fermi model in the long-wavelength limit  $y \rightarrow 0$ .

## III. ELECTROSTATIC ENERGY

### A. Uniform background

First let us outline the main results for the Coulomb crystals with the uniform background. The electrostatic

TABLE I: Madelung constant  $\zeta$  in Eq. (9) and coefficient  $\eta_{\text{TF}}$  of the quadratic approximation (15) for the bcc, fcc, hcp, and  $\text{MgB}_2$  lattice types.

lattice	$\zeta$	$\eta_{\text{TF}}$
bcc	-0.895929255682	-0.103732333707
fcc	-0.895873615195	-0.103795687531
hcp	-0.895838120459	-0.103809851801
$\text{MgB}_2$	-0.89450562823	-0.104080616256

energy of such crystals can be written as

$$U_M = N \frac{Z^2 e^2}{a} \zeta, \quad (9)$$

where  $\zeta$  is called a Madelung constant, and  $N$  is the total number of ions. Accurate values of the Madelung constant for four lattices with the lowest  $U_M$  are quoted in Table I from the previous works (see the recent review [15] and references therein).

Here we use the traditional geometry of the hcp lattice (e.g., [27]) with the distance between hexagonal layers  $h_0/2 = \sqrt{2/3} a_l \approx 0.816497 a_l$ , where  $a_l$  is the lattice constant and  $h_0$  is the height of the primitive Bravais cell, while for the one-component lattice of the  $\text{MgB}_2$  type the lowest-energy configuration is used. The electrostatic energy of the Coulomb hcp lattice is the lowest for the lattice with  $h_0/2$  replaced by  $h_{\text{min}}/2 \approx 0.81782 a_l$ , but this difference affects only the 7th significant digit of  $U_M$  and is unimportant, as we show in Sec. V below.

From Table I we see that the bcc lattice has the lowest electrostatic energy. So its formation among all lattices with one type of ion in the elementary cell and uniform background is most likely. For the multi-component crystals, formation of other lattices is also possible (e.g., [14, 15], and references therein).

## B. Polarized background. Basic notations

Expressions for the electron screening corrections to the thermodynamic functions of the one-component plasmas have been derived in frames of the thermodynamic perturbation theory by Galam and Hansen [28]. In the particular case of the one-component Coulomb crystal in the harmonic approximation, the polarization correction to the electrostatic energy can be written as [20]

$$\Delta U_{\text{pol}} = N \frac{Z^2 e^2}{a} \frac{3}{2N_{\text{cell}}^2} \sum_m' \frac{1}{(G_m a)^2} \left[ \frac{1}{\epsilon(G_m)} - 1 \right] \times \sum_{p,p'} e^{i\mathbf{G}_m(\mathbf{x}_p - \mathbf{x}_{p'})}, \quad (10)$$

where  $N_{\text{cell}}$  is the number of ions in the elementary cell and the sums run over all basis vectors  $\mathbf{x}_p$  in the elementary cell ( $p$  and  $p'$ ) and all reciprocal lattice vectors  $\mathbf{G}_m$  with the exception of  $G = 0$ . The total electrostatic

energy with the polarization correction becomes

$$U = U_M + \Delta U_{\text{pol}}. \quad (11)$$

Three approximations for the dielectric function, given by Eqs. (6), (7), and (8), yield three different values of electrostatic energy, which we denote  $U_{\text{TF}}$ ,  $U_L$  and  $U_J$ , respectively.

Equation (1) is written in the linear response approximation, which is valid if the typical energy of electron-ion interaction  $Ze^2/a$  is small compared to the Fermi energy  $E_F$ . Since

$$\frac{Ze^2/a}{E_F} = \frac{x^2}{\gamma(\gamma-1)} \frac{(\kappa_{\text{TF}} a)^2}{3^{4/3}} < 0.463 (\kappa_{\text{TF}} a)^2, \quad (12)$$

the condition  $Ze^2/a \ll E_F$  is satisfied to a good accuracy, provided that  $\kappa_{\text{TF}} a \lesssim 1$ . This condition is usually well fulfilled in the crystallized regions of the degenerate stars. It justifies that  $\epsilon(q)$  in Eq. (1) contains only polarization corrections proportional to  $\kappa_{\text{TF}}^2$ . Higher order corrections to the dielectric function are unknown. To estimate a possible effect of the higher-order terms, we expand the electrostatic energy in a series in powers of  $\kappa_{\text{TF}} a$  up to the quadratic terms. Then Eq. (10) is reduced to

$$U_{2\text{pol}} = -N \frac{Z^2 e^2}{a} (\kappa_{\text{TF}} a)^2 \times \frac{3}{2N_{\text{cell}}^2} \sum_m' \frac{\epsilon_2(G_m)}{(G_m a)^4} \sum_{p,p'} e^{i\mathbf{G}_m(\mathbf{x}_p - \mathbf{x}_{p'})}. \quad (13)$$

Energies  $U_2 \equiv U_M + U_{2\text{pol}}$  are denoted further in the text as  $U_{2J}$ ,  $U_{2L}$  and  $U_{2\text{TF}}$  for the Thomas-Fermi, Lindhard, and Jancovici models, respectively.

## C. Thomas-Fermi model

The Thomas-Fermi model is the simplest and most widely used approximation for describing the effects of electron polarization. It was applied to studies of the Coulomb crystals in degenerate stars in many works (e.g., [18–20] and references therein). However, all previous investigations concerned only the bcc and fcc lattices. Here we extend the consideration to two other lattice types, hcp and  $\text{MgB}_2$ .

As can be seen from Eqs. (1), (6), (9), and (10), for each lattice type the dimensionless ratio  $U_{\text{TF}}/(NZ^2 e^2 a^{-1})$  depends only on the single parameter  $\kappa_{\text{TF}} a$ .

To obtain the electrostatic energy, as can be seen from Eq. (13), one has to calculate slowly converging sums like  $\sum_m (-1)^m G_m^{-4}$ . In the Thomas-Fermi model, this difficulty can be overcome by the Ewald rearrangement

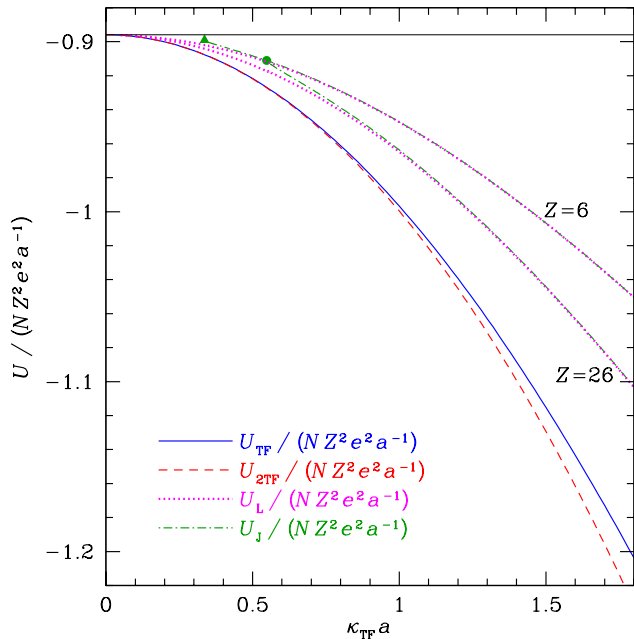


FIG. 1: Electrostatic energy of the bcc lattice in units of  $NZ^2e^2/a$  in different approximations. The full Thomas-Fermi approximation  $U_{\text{TF}}$  (Eq. (14), solid curve) and in the second-order approximation  $U_{2\text{TF}}$  (Eq. (15), dashed curve) are compared with the rigid background approximation  $U_M$  (Eq. (9), the horizontal line) and with the more accurate approximations due to Lindhard ( $U_L$ , Sec. III D, dotted lines) and Jancovici ( $U_J$ , Sec. III E, dot-dashed lines) for carbon ( $Z = 6$ ) and iron ( $Z = 26$ ). The triangle and the heavy dot mark the minimum of  $\kappa_{\text{TF}}a$  in the relativistic (Jancovici) theory for C and Fe, respectively.

[29], which reduces Eqs. (9) and (10) to

$$\begin{aligned}
 U_{\text{TF}} = NZ^2e^2 \left\{ \frac{1}{N_{\text{cell}}} \sum_{l,p,p'} (1 - \delta_{\mathbf{R}_l,0} \delta_{pp'}) \frac{E_- + E_+}{4Y_l} \right. \\
 - \frac{\kappa_{\text{TF}}}{2} \operatorname{erf} \left( \frac{\kappa_{\text{TF}}}{2\mathcal{A}} \right) - \frac{\mathcal{A}}{\sqrt{\pi}} \exp \left( -\frac{\kappa_{\text{TF}}^2}{4\mathcal{A}^2} \right) - \frac{2\pi n}{\kappa_{\text{TF}}^2} \\
 + \frac{1}{N_{\text{cell}}^2} \sum_{m,p,p'} \frac{2\pi n}{G_m^2 + \kappa_{\text{TF}}^2} \\
 \left. \times \exp \left[ -\frac{G_m^2 + \kappa_{\text{TF}}^2}{4\mathcal{A}^2} - i\mathbf{G}_m(\boldsymbol{\chi}_p - \boldsymbol{\chi}_{p'}) \right] \right\}, \quad (14)
 \end{aligned}$$

where  $E_{\pm} = e^{\pm\kappa_{\text{TF}}Y_l} \operatorname{erfc}(AY_l \pm \kappa_{\text{TF}}/(2\mathcal{A}))$ ,  $\mathbf{Y}_l = \mathbf{R}_l + \boldsymbol{\chi}_p - \boldsymbol{\chi}_{p'}$ ,  $\operatorname{erf}(x)$  is the error function,  $\operatorname{erfc}(x) \equiv 1 - \operatorname{erf}(x)$ , and  $\mathcal{A}$  is an arbitrary constant; a good numerical convergence of both sums is provided by  $\mathcal{A} \approx 2/a$  [20].

In Fig. 1, the electrostatic energy  $U$  is plotted by in different approximations for the bcc lattice. In the chosen scale, the difference between the results for different lattice types is not noticeable. In the full Thomas-Fermi model, Eq. (14), the bcc lattice has the lowest electrostatic energy at  $\kappa_{\text{TF}}a < 1.065714$ , while the fcc lattice has the lowest  $U_{\text{TF}}$  at larger  $\kappa_{\text{TF}}a$ .

The situation changes if we take the first two terms of the series expansion in the parameter  $\kappa_{\text{TF}}a$  only. This approximation gives

$$U_{2\text{TF}} = N \frac{Z^2 e^2}{a} (\zeta + \eta_{\text{TF}} (\kappa_{\text{TF}} a)^2), \quad (15)$$

where constant  $\eta_{\text{TF}}$  depends on the type of the lattice and is presented in the last column of Table I. At the selected scale in Fig. 1 the difference between  $U_{\text{TF}}$  (the solid line) and  $U_{2\text{TF}}$  (the dashed line) is noticeable only at  $\kappa_{\text{TF}}a \gtrsim 1$ . The difference between energies of different lattices is very small, and the structural transition between the bcc and fcc lattice moves from  $\kappa_{\text{TF}}a = 1.065714$  to  $\kappa_{\text{TF}}a = 0.93715$ , furthermore at  $\kappa_{\text{TF}}a > 1.58301$  the hcp lattice will possess the smallest  $U_{2\text{TF}}$ , while at  $\kappa_{\text{TF}}a > 2.21838$  the  $\text{MgB}_2$  lattice becomes more energetically preferable. However, with the exception of the bcc-fcc transition, all other transitions are outside the limits of the theory applicability.

The dotted and dot-dashed curves in Fig. 1 show the electrostatic energy in more advanced approximations, which are discussed below.

#### D. Lindhard model

The Lindhard expression for the dielectric function [22] and its generalization by Mermin [30] are widely used in the plasma physics (e.g., [28, 31]). The underlying RPA approximation makes this model more accurate than the Thomas-Fermi model.

In this case, the Ewald resummation cannot be performed explicitly. Therefore we calculate the total electrostatic energy  $U_L$  according to Eqs. (7), (10), and (11). Unlike the Thomas-Fermi model, the single parameter  $\kappa_{\text{TF}}a$  is not sufficient anymore. Since  $\epsilon_{2L}(q)$  in Eq. (7) contains an argument  $y \propto qa_e$ , the second dimensionless parameter appears,  $a_e/a$ , which equals  $Z^{-1/3}$  due to the charge neutrality. In Fig. 1, the dotted lines show  $U_L$  for carbon and iron, which are most typical chemical elements in the white dwarf cores and neutron star envelopes. In both cases the polarization correction appears smaller than in the Thomas-Fermi model. The difference  $U_L - U_{\text{TF}}$  is smaller for the larger  $Z$ , which reflects the well known fact that the Thomas-Fermi theory becomes more accurate with increasing  $Z$ .

Results for the ground-state structure are presented in Fig. 2, where the different regions hatched by the dashed lines show the range of parameters  $Z$  and  $x$  at which the fcc or hcp lattice has the lowest total energy, while the white area corresponds to the bcc lattice. The  $\text{MgB}_2$  lattice is never energetically preferred in the density range shown in this figure, where formation of Coulomb crystals can be expected in the degenerate stars. The right vertical axis displays the density parameter  $r_s$ , which is more customary than  $x$  in the nonrelativistic theory. The dot-dashed line corresponds to  $\kappa_{\text{TF}}a = 1.0657$ , which describes the structural transition between the bcc and fcc

lattices in the Thomas-Fermi model. Recalling that the linear response theory is justified at  $\kappa_{\text{TF}}a \lesssim 1$ , we should accept the results in the region below this line with caution. Anyway, we see a remarkable difference between the results obtained using the Thomas-Fermi and Lindhard models. For the latter model (unlike the former one), the ground state structure depends on  $Z$  in a nontrivial way, if the density parameter  $r_s \gtrsim 0.01$  ( $x \lesssim 1.4$ ). However, in any case the bcc lattice forms the true ground state at  $r_s < 0.01$ .

### E. Jancovici model

The Lindhard expression for the dielectric function is derived in the nonrelativistic formalism, therefore it is applicable only at  $x \ll 1$ . The Jancovici model [23] generalizes the Lindhard model taking the effects of special relativity into account. Since the relativity parameter  $x$  is not small in the crystallized regions of the most typical neutron stars and white dwarfs, the Jancovici model is more suitable in the theory of these stars (e.g., [1, 9]), although it is used relatively rarely (e.g., [20, 32, 33]). For studying the electrostatic energy it was employed only in Ref. [20] for the bcc and fcc (but not hcp) lattices.

The electrostatic energy for the Coulomb plasma of carbon and iron, calculated using the Jancovici model ( $U_J$ ), is shown in Fig. 1 by dot-dashed curves (see the data in [34]). These curves are not continued to  $\kappa_{\text{TF}}a = 0$ , because in the relativistic theory the Thomas-Fermi parameter cannot be smaller than  $(\kappa_{\text{TF}}a)_{\text{min}} = 0.185 Z^{1/3}$ , according to Eq. (5). Hence the electrostatic energy noticeably differs from the limit  $U_M$  at any density. We see that  $U_L$  and  $U_J$  are almost identical at  $\kappa_{\text{TF}}a \gtrsim 2(\kappa_{\text{TF}}a)_{\text{min}}$ , but the results of the two models substantially differ at smaller values of  $\kappa_{\text{TF}}a$ ; thus, the special relativity effects reduce the polarization correction by  $\sim 30\%$  at  $\kappa_{\text{TF}}a \sim (\kappa_{\text{TF}}a)_{\text{min}}$ .

The areas hatched with the solid lines in Fig. 2 show the ranges of parameters  $Z$  and  $x$  where the fcc or hcp lattices have the lowest electrostatic energy according to the relativistic (Jancovici) model of the dielectric function. They can be compared with the areas hatched with the dashed lines, which show analogous regions according to the nonrelativistic (Lindhard) model, which we considered in Sec. III D. The difference between these two approximations is noticeable only at  $x \sim 1$ . Qualitatively, the results are very similar. It means that the relativistic corrections to the dielectric function are not very important for the structural transitions of the Coulomb crystals. It is quite expected since the structural transitions occur mostly at  $x \lesssim 1$ . Note that relativistic corrections are rather insignificant also for the phonon spectra of Coulomb crystals [17, 20].

In Fig. 3 we plot structural transitions for the second-order approximation  $U_{2J}$ . Here,  $x$  and  $\kappa_{\text{TF}}a$  are chosen as independent parameters. Our results for the bcc and fcc lattices reproduce the results of Baiko [20]. At high  $x$  the

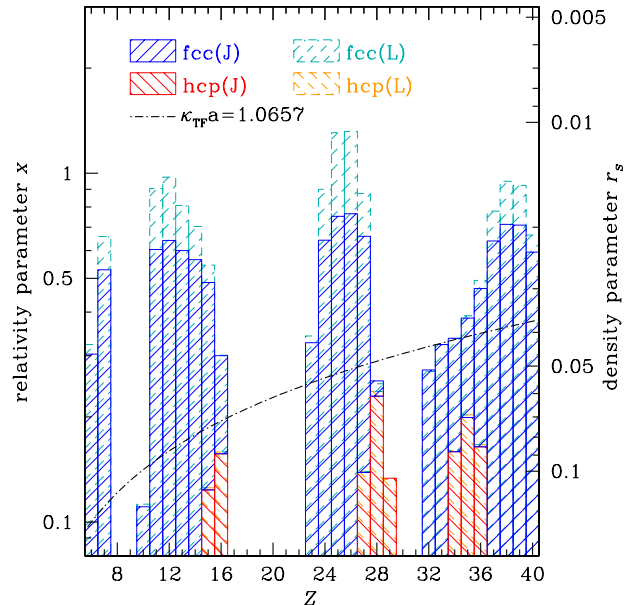


FIG. 2: The ranges of charge number  $Z$ , relativity parameter  $x$ , and density parameter  $r_s$ , at which the fcc or hcp lattice (hatched areas according to the legend) form the ground state of a classical Coulomb crystal with polarizable electron background. The dashed and solid hatchings correspond to the Lindhard and Jancovici approximations to the dielectric function of the electron background. In the white area, the ground state is formed by the bcc lattice. The dot-dashed line corresponds to  $\kappa_{\text{TF}}a = 1.065714$  and separates the regions where the ground state is bcc (above the line, where  $\kappa_{\text{TF}}a$  is smaller) or fcc (below the line, where  $\kappa_{\text{TF}}a$  is larger) in the Thomas-Fermi approximation.

transition between the bcc and fcc lattices takes place at  $\kappa_{\text{TF}}a$  between 0.935 and 0.945, which is consistent with the result of the Thomas-Fermi approximation (it gives the transition at  $\kappa_{\text{TF}}a \approx 0.93715$ ). At low densities the pattern of ground-state structures is more complicated. In the latter case, there appear several domains in the parameter plane where the hcp lattice is energetically preferable according to the Jancovici model.

## IV. ZERO-POINT VIBRATIONS

In the previous sections we did not consider zero-point quantum vibrations of ions around their equilibrium positions. This model would be accurate for very massive ions. In reality, the relative atomic weight  $A$  varies from  $A \approx 2Z$  in the outer shells of neutron star crusts or crystallized cores of white dwarfs to  $A \approx 3.5Z$  near the neutron drip point in the neutron-star crust. In this section, we consider the effects of the quantum vibrations on the ground-state structure of a Coulomb crystal, assuming  $A = 2Z$ . In this way we obtain an estimate of the upper limits for these effects, because a larger  $A$  would result in a smaller vibration energy and accordingly a smaller dif-

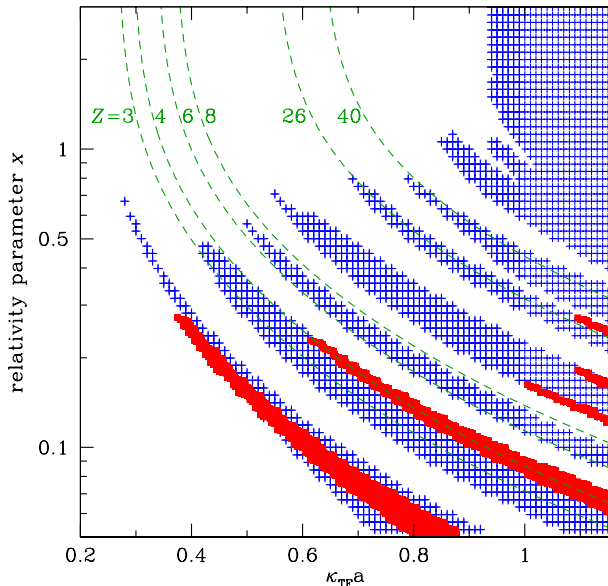


FIG. 3: The ranges of parameters  $x$  and  $\kappa_{\text{TF}}a$  at which one or another lattice has the smallest  $U_{2J}$ . The bcc lattice forms the ground state in the white region, the fcc lattice in the blue cross-hatched regions, and the hcp in the red filled regions. The dashed lines corresponds to  $Z = 3, 4, 6, 8, 26,$  and  $40$  (marked near the curves).

ference from the results obtained for the classical (fixed in space) ions.

The energy of the ground-state quantum vibrations of a three-dimensional harmonic lattice equals (cf., e.g., [24])

$$E_0 = \frac{3}{2}N\hbar\langle\omega\rangle, \quad (16)$$

where  $\langle\omega\rangle$  is the phonon frequency  $\omega_\nu(\mathbf{k})$ , averaged over all phonon modes  $\nu$  and wavevectors  $\mathbf{k}$  in the first Brillouin zone. In the first approximation, the total ground-state energy is given by the sum  $E = U + E_0$ , where  $U$  is the electrostatic energy (11). Equation (16) can be written in the dimensionless form as

$$\frac{E_0}{NZ^2e^2/a} = \frac{3}{2}\sqrt{\frac{3}{R_S}}u_1, \quad (17)$$

where  $R_S \equiv a/[\hbar/m_{\text{ion}}(Ze)^2] \approx 1823AZ^{7/3}r_s$  is the ion density parameter (analogous to  $r_s$  for the electrons),  $u_1 \equiv \langle\omega\rangle/\omega_p$ ,  $\omega_p = \sqrt{4\pi nZ^2e^2/m_{\text{ion}}}$  is the ion plasma frequency,  $m_{\text{ion}} = Am_u$  is the ion mass, and  $m_u$  is the unified atomic mass unit.

To calculate  $\langle\omega\rangle$  and thus  $u_1$ , the phonon spectrum was obtained by solving the dispersion equation, as described in Ref. [17]:  $\det\{D_{ss'}^{\alpha\beta}(\mathbf{k}) - \omega_\nu^2(\mathbf{k})\delta^{\alpha\beta}\delta_{ss'}\} = 0$ , where  $s$  and  $s'$  run over the ions in the elementary cell, and  $D_{ss'}^{\alpha\beta}(\mathbf{k})$  is the dynamic matrix. Generally,  $D_{ss'}^{\alpha\beta}(\mathbf{k})$  is given, e.g., by Eq. (5.6) of Ref. [18], but in this sec-

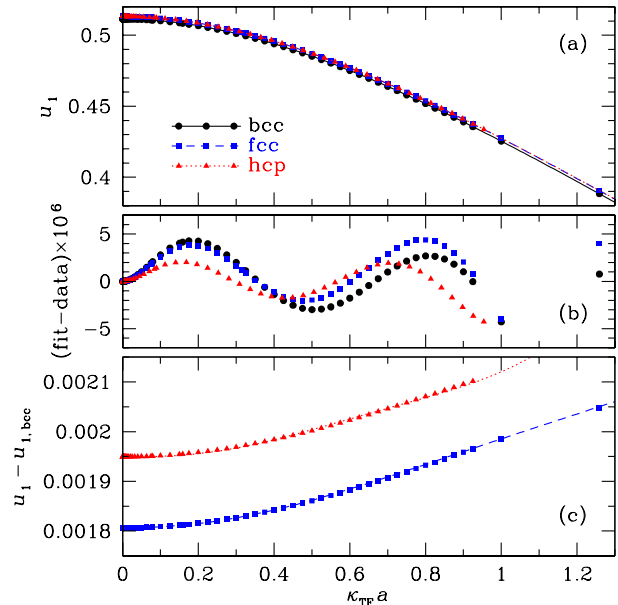


FIG. 4: *Top panel:* Dependence of the first phonon moment  $u_1$  on the Thomas-Fermi parameter: computed values (black dots, blue squares, and red triangles for the bcc, fcc, and hcp Coulomb lattices, respectively) and the analytic fit, Eq. (18) (the solid, dashed, and dotted lines, respectively). *Middle panel:* The fit residuals, multiplied by  $10^6$ . *Bottom panel:* The excess of the first phonon moment  $u_1$  for the fcc and hcp Coulomb lattice over that for the bcc lattice, calculated from the numerical results (the symbols) and the analytic fit (the lines).

tion we calculate it in the Thomas-Fermi approximation (according to Eqs. (3)–(5) of Ref. [16]).

The electron polarization decreases  $u_1$  and slightly affects the differences  $\Delta u_1$  between the different lattice types. In the Thomas-Fermi model this dependence is well described by the simple Padé approximation:

$$u_1 = \frac{u_1^0 [1 + p_4(\kappa_{\text{TF}}a)^3]}{1 + p_1(\kappa_{\text{TF}}a)^2 + p_2(\kappa_{\text{TF}}a)^4 + p_3(\kappa_{\text{TF}}a)^6}, \quad (18)$$

where  $u_1^0$  is the value of  $u_1$  in the one-component plasma model with the rigid background and  $p_i$  are fitting parameters, which are given in Table II. The computed and fitted dependencies of  $u_1$  on  $\kappa_{\text{TF}}a$  are shown in Fig. 4. The residuals between the fit, Eq. (18), and the numerical results are smaller than  $5 \times 10^{-6}$  (see the middle panel of Fig. 4), which provides a good analytic approximation to the differences  $\Delta u_1$ , which are typically a few times  $10^{-3} - 10^{-4}$  in this approximation (the bottom panel).

The zero-point energy given by Eqs. (16) and (18) was added to the electrostatic energy, computed according to Eqs. (10) and (9), to obtain the total ground-state energy  $E$  of a Coulomb crystal. Its absolute ground state is formed by the lattice that delivers the lowest ground-state energy. The results of this evaluation are shown in Fig. 5. Here we have assumed  $A = 2Z$ . A larger value of

TABLE II: Parameters of Eq. (18).

lattice	$u_1^0$	$p_1$	$p_2$	$p_3$	$p_4$
bcc	0.5113874	0.246236	0.05496	0.0026	0.08457
fcc	0.5131940	0.244996	0.05490	0.0025	0.08463
hcp	0.5133369	0.245250	0.05663	0.0021	0.08599

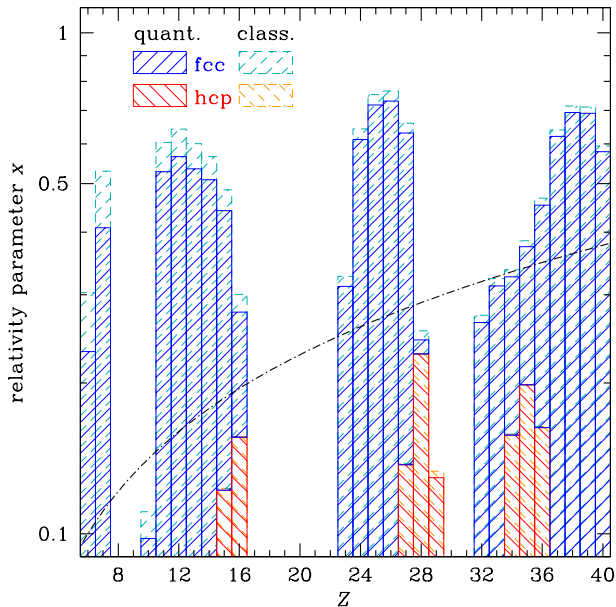


FIG. 5: The same as in Fig. 2, but taking the zero-point ion vibrations into account (solid lines and hatched areas). For comparison, the dashed lines and dashed hatched areas show the results without the zero-point vibrations. The Jancovici model for the electron dielectric function is used in all the cases.

A would lead to smaller differences from the classical-ion model, whose results are also reproduced in this figure. We see that the zero-point vibrations almost do not affect the boundaries of the hcp domain. They somewhat decrease the densities of the fcc/bcc transition, but this effect is not profound; it is even smaller than the one due to the special relativity corrections (cf. Fig. 3).

## V. POSSIBLE SMALL CORRECTIONS

One may note that the results presented in Figs. 4 and 5 rely on the dependence of  $u_1$  on the polarization parameter  $\kappa_{\text{TF}}a$  obtained using the Thomas-Fermi model, which results in the one-parameter dependence  $u_1(\kappa_{\text{TF}}a)$ . A more accurate (e.g., Lindhard or Jancovici) model gives a two-parametric dependence  $u_1(\kappa_{\text{TF}}a, x)$ . An example of the bcc Coulomb lattice at  $\kappa_{\text{TF}}a = 0.5$  presented in Ref. [35] indicates that the difference of the first phonon moment in the Thomas-Fermi approximation  $u_1$  relative to its rigid-background value  $u_1^{(0)}$  may be slightly smaller in the Jancovici model than in the

Thomas-Fermi model. It is difficult to evaluate the differences between  $\Delta u_1$  between the different lattice types beyond the Thomas-Fermi approximation with the accuracy that is needed to determine the effect on the boundaries between different ground-state lattice types, but the rough estimation for  $\kappa_{\text{TF}}a = 0.5$  shows that  $u_1$  of the fcc lattice is greater than the  $u_1$  of the bcc lattice at any  $x$ . For instance, at  $x = 1$   $u_{1,\text{bcc}} \approx 0.48587$  while  $u_{1,\text{fcc}} \approx 0.48686$ . Hence we expect that the  $x$ -dependence of  $u_1$  cannot qualitatively change the results presented in Fig. 5. To check the last statement, we repeated our calculations in the extreme case, where the polarization dependence of  $u_1$  is completely suppressed (i.e.,  $u_1 = u_1^{(0)}$ ) and found that the boundaries between different structural phases in Fig. 5 shift no more than by  $\Delta \log_{10} x \lesssim 0.0065$ , provided that  $x \gtrsim 0.1$ , which means that the densities of phase boundaries vary by less than 1.5%. Clearly, such small shift of the boundary cannot have any observable consequence, so that it is safe to use Eq. (16) with the one-parametric expression (18) for evaluation of the zero-point ion vibrations energy.

As mentioned above, in the bulk of our numerical calculations we fixed the height of the primitive cell in the hcp lattice at  $h_0 = \sqrt{8/3}a_l$ . However, the true minimum of the electrostatic energy  $U(h)$  as a function of the cell height  $h$  is reached at a slightly larger height value,  $h_{\text{min}}$ . In the Thomas-Fermi approximation for the polarizable electron background,  $h_{\text{min}}$  slowly decreases with increasing  $\kappa_{\text{TF}}a$  and can be reproduced at  $\kappa_{\text{TF}}a \lesssim 3$  by the fitting expression

$$h_{\text{min}} \approx h_0 + 0.00265 \left\{ 1 - \frac{0.155 (\kappa_{\text{TF}}a)^2}{1 + 0.11 (\kappa_{\text{TF}}a)^2} \right\}. \quad (19)$$

The corresponding difference in the ground-state energy is described by the fit

$$\Delta\zeta_h \equiv \frac{U(h_{\text{min}}) - U(h_0)}{NZ^2e^2/a} \approx -3.3 \times 10^{-7} \exp \left[ -\frac{(\kappa_{\text{TF}}a)^2}{2} \right]. \quad (20)$$

At  $\kappa_{\text{TF}}a \lesssim 3$  these expressions provide the absolute accuracy within  $\sim 10^{-5}$  for  $h_{\text{min}}$  and within  $\sim 5 \times 10^{-9}$  for  $\Delta\zeta_h$ . This correction shifts the densities of transitions between different ground-state structural phases in Figs. 2 and 5 by  $\lesssim 0.7\%$ .

The MgB<sub>2</sub> lattice has a similar insignificant dependence  $h_{\text{min}}$  on  $\kappa_{\text{TF}}a$  (see discussion in Ref. [21]).

## VI. DISCUSSION AND CONCLUSIONS

We used and compared several theoretical models to study the influence of the polarization of degenerate electron background to the electrostatic properties of Coulomb crystals and to their structure in the neutron star crusts and white dwarf interiors.

The studies of the electrostatic energies of Coulomb crystals with uniform background appear to be quite complete now, as presented in the review [15]. Based

on the results of Ref. [15], we chose four lattices with the lowest Madelung constant (bcc, fcc, hcp and  $\text{MgB}_2$ ) and investigated polarization effects for them. Since the  $\text{MgB}_2$  lattice never has the lowest energy the formation of other lattices, which were not considered in the present work, is very unlikely.

The Thomas-Fermi model predicts that at  $\kappa_{\text{TFA}} < 1.065714$  the bcc lattice forms the ground state, while at higher  $\kappa_{\text{TFA}}$  the fcc lattice is energetically preferable. The Thomas-Fermi model, as well as the linear response theory in general, allows one to obtain only corrections  $\sim (\kappa_{\text{TFA}})^2$ . Our estimate of the effect of the higher order corrections shows that they can noticeably change the general picture of structural transitions. For instance, omitting all higher order corrections to the electrostatic energy within the Thomas-Fermi model leads to the shift of the transition between bcc and fcc lattice to  $\kappa_{\text{TFA}} \approx 0.93715$ , while at  $\kappa_{\text{TFA}} \approx 1.58301$  transition between the fcc and hcp lattices appear.

The Lindhard and Jancovici RPA-based models give quite similar results as concerns the ground-state lattice structure, which qualitatively differ from the Thomas-Fermi approximation. Instead of a single structural transition from the bcc to fcc lattice, a strong nontrivial dependence on the charge number  $Z$  appears. In addition, it the hcp lattice can form the ground state for some  $Z$  at relatively low density. The relativistic corrections to the dielectric function, given by the Jancovici model, as well as the quantum corrections due to zero-point vibrations of ions, only moderately shift the structural transition densities. In all considered models, the bcc lattice possesses the lowest electrostatic energy at the density parameters  $r_s < 0.01$  (mass densities  $\rho \gtrsim 5 \times 10^6 \text{ g cm}^{-3}$ ) for any  $Z$ . In the most advanced of the models (Fig. 5), the unconditional bcc stability range extends down to the relativity parameters  $x \gtrsim 0.8$  (mass densities  $\rho \gtrsim 10^6 \text{ g cm}^{-3}$ ).

As shown in Ref. [21], the equation for the electrostatic energy of the Coulomb crystal with the Thomas-Fermi dielectric function is almost the same as the equation for the electrostatic energy of the Yukawa crystal, which is a usual model for ordered dusty plasmas [6, 8, 36–39]. A slight difference is that in the Yukawa crystal the screening parameter is the Debye wavenumber  $\kappa_D$  and there is no restriction analogous to  $\kappa_{\text{TFA}} \lesssim 1$ . The Yukawa crystal model is used up to  $\kappa_D a = 4.76$ , when it becomes unstable against phonon oscillations [21, 40]. Hence both systems have the same structural transitions. Thus, while in the Lindhard model at  $\kappa_{\text{TFA}} \gtrsim 1$  the fcc and hcp lattices become energetically preferable and the strong dependence of structural transitions on  $Z$  appears, we can expect a similar situation if higher order corrections to the Yukawa crystal model are taken into account. Since in the dusty plasmas it is impossible to maintain strictly the same charge for all grains, the formation of the hcp-fcc crystal mixture is more likely.

The appearance of the hcp ground state at sufficiently large  $\kappa_{\text{TFA}}$  in the linear response theory may be a key

to explanation of data of the experiment KPT-10 “Kulonovskiy Kristall” (“Coulomb Crystal”) onboard the International Space Station. This experiment has revealed that dusty particles with  $\kappa_D a = 0.5 - 3$  form an ordered system with the hcp and fcc structures (e.g., [41, 42]). Since equations for the electrostatic energy of the Coulomb crystal with the Thomas-Fermi dielectric function and of the Yukawa crystal are the same, it makes sense to assume that for systems with a non-degenerate background (such as the dusty crystals) the higher order screening corrections may bring us to the situation similar to the degenerate case, which is described above, where the fcc and hcp lattices may form the ground state.

It may be of interest for the reader to note that, beside the dusty plasmas mentioned above, the normal electron-hole plasmas in semiconductors also demonstrate some similarities to the dense ion-electron plasmas. The crystallization of the electron-hole plasmas with heavy holes was studied in Refs. [43, 44], using the path integral Monte Carlo simulations.

Back to degenerate stars, let us note that our reported model improvements are likely unimportant for the ground-state equation of state or chemical composition. Previously, Chamel and Fantina [45] studied this problem based on the Thomas-Fermi model of electron polarization, scaled so as to approach the more accurate polarization results of Ref. [19]. In particular, Chamel and Fantina found that corrections to the electron-capture threshold in white-dwarf cores are very small and the neutron-drip density and pressure in the crusts of neutron stars are only slightly shifted. Although electron polarization may change the composition of the crust of nonaccreting neutron stars, uncertainties in the masses of neutron-rich isotopes were found to be more important than electron exchange and polarization effects. As can be seen from our Fig. 1, the polarization correction to the energy has the same order of magnitude in the Thomas-Fermi model as in the more accurate Lindhard and Jancovici models. Therefore, these improvements in the model cannot qualitatively change the conclusions by Chamel and Fantina [45]. Let us also note that some modern neutron-star equations of state take sufficiently accurate account of the electron polarization effects (e.g., Ref. [46]).

On the other hand, our results show that the replacement of the traditional Thomas-Fermi model by the RPA-based models of the polarization corrections can strongly shift the boundaries between the bcc and fcc lattice types and lead to appearance of the hcp lattices in the cores of white dwarfs and crusts of neutron stars. The interfaces between different lattice structures may affect the kinetic properties of the crust. For example, crust failure due to accumulated stresses during neutron-star evolution (e.g., Refs. [47–49]) can likely develop along the surfaces separating the different lattice types, where the breaking stress can be smaller than its standard value in the bulk of the crust [50].

Based on the presented results, we can conclude that



the most part of the crust of neutron stars and crystallized cores of white dwarfs at  $\rho \gtrsim 10^6$  g/cm<sup>3</sup> consist of the bcc lattice at any  $Z$ , which is the standard assumption for their modeling. At lower densities, however, the fcc and hcp lattices can form the true ground state. Crystallization of the one-component plasma occurs at  $\Gamma \approx 175$ , where  $\Gamma \equiv Z^2 e^2 / (ak_B T) = 22.5 Z^{5/3} x / T_6$  is the Coulomb coupling parameter,  $T$  is temperature,  $T_6 \equiv T / 10^6$  K, and  $k_B$  is the Boltzmann constant [19]. This implies  $T \lesssim 1.3 \times 10^5 Z^{5/3} x$  K, which leads to  $T \lesssim (3 \times 10^7) x$  K for an envelope of a neutron star composed of iron or nickel or  $T \lesssim (2.5 \times 10^6) x$  K for a carbon plasma in a white dwarf or in an accreted crust of a neutron star. Taking the electron polarization into account, one finds that the crystallization may occur at somewhat smaller  $\Gamma$  (larger  $T$ ) [51]. Hence the Coulomb crystals can exist in the degenerate stars not only at  $x \gtrsim 1$ , but also in the nonrelativistic ( $x < 1$ ) parts of envelopes of sufficiently old and cold neutron stars (see, e.g., Fig. 2.2. in Ref. [9]) or white dwarfs (e.g., Fig. 4 in Ref. [52]), where one can anticipate formation of the fcc and hcp structures.

However, the smallness of energy differences between

these structures makes it possible that thermal fluctuations destroy the long-range order at the temperature of crystallization and thus make the structure of some domains out of the true ground state. Therefore, the neutron star crust and white dwarf matter at such low densities and temperatures may consist of polycrystalline mixtures of different types of lattices or even amorphous solid. Beside the influence on the elastic and breaking properties of the crust, the presence of polycrystalline or amorphous structures can suppress the electrical and thermal conductivities, causing observable consequences for the magnetic and thermal evolution of a neutron star. This possibility deserves a further study.

### Acknowledgments

This research was supported by The Ministry of Science and Higher Education of the Russian Federation (Agreement with Joint Institute for High Temperatures RAS No. 075-15-2020-785).

- 
- [1] D. G. Yakovlev and D. A. Shalybkov, Degenerate cores of white dwarfs and envelopes of neutron stars: thermodynamics and plasma screening in thermonuclear reactions, *Sov. Sci. Rev., Ser. E: Astrophys. Space Phys. Rev.* **7**, 311 (1989).
  - [2] V. Fortov, *Thermodynamics and Equations of State for Matter: From Ideal Gas to Quark-Gluon Plasma* (World Scientific, 2016).
  - [3] W. Ebeling, V. Fortov, and V. Filinov, *Quantum Statistics of Dense Gases and Nonideal Plasmas* (Springer, 2017).
  - [4] M. Born and K. Huang, *Dynamical Theory of Crystal Lattices* (Oxford University Press, Oxford, 1954).
  - [5] S.L. Shapiro, and S.A. Teukolsky, *Black Holes, White Dwarfs, and Neutron Stars* (Wiley-Interscience, New York, 1983).
  - [6] V. E. Fortov, A. G. Khrapak, S. A. Khrapak, V. I. Molotkov and O. F. Petrov, Dusty plasmas, *Phys. Usp.* **47**, 447 (2004).
  - [7] C. Kittel, *Introduction to Solid State Physics* (Wiley, Hoboken, 2004).
  - [8] V. E. Fortov, A. V. Ivlev, S. A. Khrapak, A. G. Khrapak, and G. E. Morfill, Complex (dusty) plasmas: Current status, open issues, perspectives, *Phys. Rep.* **421**, 1 (2005).
  - [9] P. Haensel, A. Y. Potekhin, and D. G. Yakovlev, *Neutron Stars 1: Equation of State and Structure* (Springer, New York, 2007).
  - [10] L. G. Althaus, A. H. Corsico, J. Isern, and E. Garcia-Berro, Evolutionary and pulsational properties of white dwarf stars, *Astron. Astrophys. Rev.* **18**, 471 (2010).
  - [11] M. Bonitz, P. Ludwig, H. Baumgartner, et al., Classical and quantum Coulomb crystals, *Physics of Plasmas* **15**, 055704 (2008).
  - [12] H. M. van Horn, The crystallization of white dwarf stars, *Nature Astronomy* **3**, 129 (2019).
  - [13] D. A. Baiko, A. Y. Potekhin, and D. G. Yakovlev, *Phys. Rev. E* **64**, 057402 (2001).
  - [14] N. Chamel and A.F. Fantina, Binary and ternary ionic compounds in the outer crust of a cold nonaccreting neutron star, *Phys. Rev. C* **94**, 065802 (2016).
  - [15] A.A. Kozhberov, Electrostatic properties and stability of Coulomb crystals, *Contrib. Plasm. Phys.* **60**, e202000021 (2020).
  - [16] A.A. Kozhberov and D.A. Baiko, Physical features of binary Coulomb crystals: Madelung energy, collective modes and phonon heat capacity, *Contrib. Plasm. Phys.* **52**, 153 (2012).
  - [17] A. A. Kozhberov, Structure and thermodynamic properties of Coulomb crystals in interiors of degenerate stars, *Ph.D. Thesis*, Ioffe Institute, Saint Petersburg, 2018.
  - [18] E. L. Pollock and J.P. Hansen, Statistical mechanics of dense ionized matter. II. Equilibrium properties and melting transition of the crystallized one-component plasma, *Phys. Rev. A* **8**, 3110 (1973).
  - [19] A. Y. Potekhin and G. Chabrier, Equation of state of fully ionized electron-ion plasmas. II. Extension to relativistic densities and to the solid phase, *Phys. Rev. E* **62**, 8554 (2000).
  - [20] D. A. Baiko, Effect of the electron gas polarizability on the specific heat of phonons in Coulomb crystals, *Phys. Rev. E* **66**, 056405 (2002).
  - [21] A. A. Kozhberov, Electrostatic energy and phonon properties of Yukawa crystals, *Phys. Rev. E* **98**, 063205 (2018).
  - [22] J. Lindhard, On the properties of a gas of charged particles, *Kgl. Danske Videnskab. Selskab, Mat.-Fys. Medd.* **28**, 8 (1954).
  - [23] B. Jancovici, On the relativistic degenerate electron gas, *Nuovo Cim.* **25**, 428 (1962).

- [24] N. W. Ashcroft and N. D. Mermin, *Solid State Physics* (Thomson Learning, Toronto, 1976).
- [25] W. B. Hubbard and W. L. Slattery, Statistical mechanics of light elements at high pressure. I. Theory and results for metallic hydrogen with simple screening, *Astrophys. J.* **168**, 131 (1971).
- [26] E. E. Salpeter, Energy and pressure of a zero-temperature plasma, *Astrophys. J.* **134**, 669 (1961).
- [27] T. Nagai and H. Fukuyama, Ground state of a Wigner crystal in a magnetic field. II. Hexagonal close-packed structure, *J. Phys. Soc. Japan* **52**, 44 (1983).
- [28] S. Galam and J.-P. Hansen, Statistical mechanics of dense ionized matter. VI. Electron screening corrections to the thermodynamic properties of the one-component plasma, *Phys. Rev. A* **14**, 816 (1976).
- [29] P. Ewald, Die Berechnung Optischer und Elektrostatistischer Gitterpotentiale, *Annalen der Physik* **369**, 253 (1921).
- [30] N. D. Mermin, Lindhard dielectric function in the relaxation-time approximation, *Phys. Rev. B* **1**, 2362 (1970).
- [31] T. Dornheim, S. Groth, and M. Bonitz, The uniform electron gas at warm dense matter conditions, *Phys. Rep.* **744**, 1 (2018).
- [32] A. Y. Potekhin, D. A. Baiko, P. Haensel, and D. G. Yakovlev, Transport properties of degenerate electrons in neutron star envelopes and white dwarf cores, *Astron. Astrophys.*, **346**, 345 (1999).
- [33] J. Daligault and S. Gupta, Electron-ion scattering in dense multi-component plasmas: Application to the outer crust of an accreting neutron star, *Astrophys. J.* **703**, 994 (2009).
- [34] Supplemental Material (file `supplement.txt`) presents the computed polarization correction  $\Delta U_{\text{pol}}$  to the electrostatic energy of the classical bcc, fcc, and hcp Coulomb crystals on the polarizable electron background in the Jancovici model.
- [35] A. A. Kozhberov, Properties of magnetized Coulomb crystals of ions with polarizable electron background, *Phys. Plasmas* **25**, 062706 (2018).
- [36] R. T. Farouki and S. Hamaguchi, Thermal energy of the crystalline one-component plasma from dynamical simulations, *Phys. Rev. E* **47**, 4330 (1993).
- [37] S. Hamaguchi and R. T. Farouki, Thermodynamics of strongly-coupled Yukawa systems near the one-component-plasma limit. I. Derivation of the excess energy, *J. Chem. Phys.* **101**, 9876 (1994).
- [38] R. T. Farouki and S. Hamaguchi, Thermodynamics of strongly-coupled Yukawa systems near the one-component-plasma limit. II. Molecular dynamics simulations, *J. Chem. Phys.* **101**, 9885 (1994).
- [39] S. Hamaguchi, R. T. Farouki, and D. H. E. Dubin, Triple point of Yukawa systems, *Phys. Rev. E* **56**, 4671 (1997).
- [40] M. O. Robbins, K. Kremer, and G. S. Grest, Phase diagram and dynamics of Yukawa systems, *J. Chem. Phys.* **88**, 3286 (1988).
- [41] B. Klumov, G. Joyce, C. R ath, P. Huber, H. Thomas, G. E. Morfill, V. Molotkov, and V. Fortov, Structural properties of 3D complex plasmas under microgravity conditions, *Europhys. Lett.* **92**, 15003 (2010).
- [42] B. A. Klumov, On melting criteria for complex plasma, *Phys. Usp.* **53**, 1053 (2010).
- [43] V. Filinov, M. Bonitz, V. Fortov, H. Fehske, and P. Levashov, Coulomb crystal and quantum melting in electron-hole plasmas of semiconductors under high pressure, *Phys. Stat. Sol. B* **244**, 474 (2007).
- [44] V. S. Filinov, H. Fehske, M. Bonitz, V. E. Fortov, and P. Levashov, Correlation effects in partially ionized mass asymmetric electron-hole plasmas, *Phys. Rev. E* **75**, 036401 (2007).
- [45] N. Chamel and A.F. Fantina, Electron exchange and polarization effects on electron captures and neutron emissions by nuclei in white dwarfs and neutron stars, *Phys. Rev. D* **93**, 063001 (2016).
- [46] J. M. Pearson, N. Chamel, A. Y. Potekhin, A. F. Fantina, C. Ducoin, A. K. Dutta, and S. Goriely, Unified equations of state for cold non-accreting neutron stars with Brussels-Montreal functionals. I. Role of symmetry energy, *Mon. Not. R. Astron. Soc.* **481**, 2994 (2018); erratum: *Mon. Not. R. Astron. Soc.* **486**, 768 (2019).
- [47] M. Ruderman, Neutron Star Crustal Plate Tectonics. III. Cracking, Glitches, and Gamma-Ray Bursts, *Astrophys. J.* **382**, 587 (1991).
- [48] G. Ushomirsky, C. Cutler, and L. Bildsten, Deformations of accreting neutron star crusts and gravitational wave emission, *Mon. Not. R. Astron. Soc.* **319**, 902 (2000).
- [49] S. K. Lander and K. N. Gourgouliatos, Magnetic-field evolution in a plastically failing neutron-star crust, *Mon. Not. R. Astron. Soc.* **486**, 4130 (2019).
- [50] A. A. Kozhberov and D. G. Yakovlev, Deformed crystals and torsional oscillations of neutron star crust, *Mon. Not. R. Astron. Soc.* **498**, 5149 (2020).
- [51] A. Y. Potekhin and G. Chabrier, Equation of state for magnetized Coulomb plasmas, *Astron. Astrophys.* **550**, A43 (2013).
- [52] F. D'Antona and I. Mazzitelli, Cooling of white dwarfs, *Annu. Rev. Astron. Astrophys.* **28**, 139 (1990).